Spin and Dielectric Transitions Promoted by Dimerization of Anionic Radical Stack and Volume-conserving Motion of Cations in an Ion-pair Compound

Zi-Heng Feng,[a] Qin-Yu Zhu,[a] Yin Qian,*[a] Xu-Sheng Gao,*[a] Xiao-Ming Ren*[a,b]

[a]State Key Laboratory of Materials-Oriented Chemical Engineering and College of Chemistry and Molecular Engineering, Nanjing Tech University, Nanjing 211816, P. R. China

[b]State Key Laboratory of Coordination Chemistry, Nanjing University, Nanjing 210023, P. R. China

Email:

yinqian@njtech.edu.cn (Y.Q.)

gaoxs@njtech.edu.cn (X.S.G.)

xmren@njtech.edu.cn (X.M.R.)

Contents

Experimental section

Reagents and materials

Preparation of compounds

Physical measurements

X-ray Crystallography

References

Experimental section

Reagents and materials

All reagents and materials of analytical grade were obtained from commercial sources and used without additional purification. Disodium maleonitriledithiolate (Na$_2$mnt) was synthesized according to published procedures.[1]

Synthesis of [DPIm][Ni(mnt)$_2$] (1)

A solution containing NiCl$_2$·6H$_2$O (0.237 g, 0.01 mol) and Na$_2$mnt (0.37 g, 0.02 mol) in H$_2$O was stirred for 2 hours, followed by the addition of [DPIm]Br (0.451 g, 0.02 mol). The resulting red microcrystals were filtered, washed with H$_2$O, and subsequently dried under vacuum. The red microcrystals were dissolved in methanol, and to this solution, a solution of I2 in methanol was added. After stirring for 2 hours, the resulting black microcrystals were harvested by filtration, washed with methanol, and dried under vacuum. Yield: ~62% (Found: C, 41.36; H, 3.55; N, 17.11%. Calc. for C$_{14}$H$_{11}$N$_6$NiS$_4$: C, 41.47; H, 3.48; N, 17.07%). Selected Infrared spectrum bands (cm^{-1}): 2207(vs) is attributed to the $\nu_{C\equiv N}$ of the mnt^{2-} ligands; 2977(s) and 3111(w)corresponding to ν_{C-H} in the imidazole rings and both methyl and methylene; 1564(s) is assigned to the skeleton vibration in imidazole rings; 1161(vs) and 1456(s) arise from the $\nu_{C=S} + \nu_{C=C}$ and ν_{C-C} of the mnt^{2-} ligands.

Chemical and Physical Measurement

Elemental analyses for C, H and N were performed with an Elementar Vario EL III analytical instrument. Infrared spectra (IR) were recorded on a Nicolet iS5 spectrometer with KBr pellets in the spectral range of 400−4000 cm^{-1}. The powder X-ray diffraction (PXRD) patterns were collected using a SHIMADZU XRD-6100 diffractometer with Cu Kα radiation ($\lambda = 1.5418$ Å), operated at 40 kV and 40 mA. The 2θ angle ranges from 5 to 50° with a step of 0.01° at ambient condition. Thermogravimetric analysis (TGA) was performed with an SDT Q600 thermogravimetric analyzer in 20-800 °C under nitrogen atmosphere, the polycrystalline sample was placed in a platinum-pan, the heating rate is 20 °C min^{-1} and the nitrogen flow rate is 100 mL min^{-1}. Differential scanning calorimetry (DSC) was carried out for **1** on a Pyris 1 power-compensation differential scanning calorimeter with a warming rate of 10 K min^{-1} during the heating

process. Optical graphs were observed with a Leica DMRX polarizing optical microscope equipped with a LINKAM LTS350 cool and hot stage. Magnetic susceptibility data were measured for polycrystalline samples on a Quantum Design MPMS-5 superconducting quantum interference device magnetometer, such a measurement was performed over the temperature range of 1.8−400 K in both cooling and warming modes and in the applied magnetic field of 2000 Oe, and the diamagnetism arising from atomic cores has been removed. Temperature- and frequency-dependent dielectric permittivity and AC impedance measurements were carried out on a Concept 80 system (Novocontrol, Germany) in 273−373 K for **1**, respectively. The powdered disc, with a thickness of ca. 1.585 mm as well as a diameter of 7.0 mm, was coated by gold films on the opposite surfaces and sandwiched by platinum electrodes and the AC frequencies span from 100 to 10^7 Hz. The X-ray single crystal crystallography information files of 1 in LTP and HTP were used as the input file. In Crystal Explorer, the electrostatic potential surface map was calculated using the TONTO application with B3LYP/6-311G (d,p) ± 0.03 a.u. For HTP, the crystal symmetry was reduced to $P2_12_12_1$ to remove the symmetry-disordered cations.

X-ray Crystallography

Single crystal X-ray diffraction (SCXRD) data for **1** were collected at 173 K using Graphite monochromated Mo Kα (λ = 0.71073 Å) on a Bruker D8 QUEST Apex III CCD area detector diffractometer. Data reduction and absorption correction were performed with the SAINT[2] and SADABS[3] software packages, respectively. The structures were solved by a direct method using the SHELXL-2018 software package4. The non-hydrogen atoms were anisotropically refined using the full-matrix least-squares method on F^2. All hydrogen atoms were geometrically fixed and placed in the ideal position.

Table S1: Crystallographic data and refinement parameters of **1** at 298 and 368 K

Chemical formula	$C_{17}H_{17}N_6NiS_4$	$C_{17}H_{17}N_6NiS_4$
Temperature / K	298	368
CCDC number	2076780	2076781
Formula weight	492.32	492.32
Crystal system	Monoclinic	Orthorhombic
Wavelength/Å	0.71073	0.71073
Space group	$P2_1/n$	$Pnma$
a / Å	7.1823(4)	20.09(7)
b / Å	20.787(14)	7.18(2)
c / Å	15.2194(10)	16.16(5)
α / °	90	90
β / °	96.373(3)	90
γ / °	90	90
V (Å^3) / Z	2258.2(2) / 4	2331(13) /4
ρ / g cm^{-3}	1.448	1.403
F(000)	1012	1012
θ Ranges	2.38−27.54	2.38−14.997
Index range	−9 ≤ h ≤ 9,	0 ≤ h ≤ 14,
	−22 ≤ k ≤ 26,	0 ≤ k ≤ 5,
	−19 ≤ l ≤ 16	0 ≤ l ≤ 11
Goodness-of-fit on F^2	0.915	1.086
[a]R$_1$, [b]wR$_2$ [I>2σ(I)]	0.0584, 0.1286	0.0889, 0.2217
R$_1$, wR$_2$ [all data]	0.1709, 0.1754	0.1341, 0.2692

[a]$R_1 = \sum||Fo| - |Fc|/\sum|Fo|$; [b]$wR_2 = \{\sum[w(Fo^2 - Fc^2)^2]/\sum[w(Fo^2)^2]\}^{1/2}$

Table S2 Selected bond lengths and angles in anion and cation of **1** at 298 and 368 K

Bond lengths /Å

T = 298 K		T = 368 K	
Ni(1)-S(1)	2.1462(13)	Ni(1)-S(1)	2.135(13)
Ni(1)-S(2)	2.1455(13)	Ni(1)-S(2)	2.128(13)
Ni(1)-S(3)	2.1413(13)	Ni(1)-S(3)	2.121(13)
Ni(1)-S(4)	2.1421(12)	Ni(1)-S(4)	2.132(12)
S(1)-C(1)	1.714(5)	S(1)-C(1)	1.66(6)
S(2)-C(2)	1.705(5)	S(2)-C(2)	1.75(7)
S(3)-C(5)	1.700(4)	S(3)-C(5)	1.70(6)
S(4)-C(6)	1.703(4)	S(4)-C(6)	1.71(6)
N(2)-C(4)	1.141(6)	N(2)-C(4)	1.24(5)
C(2)-C(1)	1.370(6)	C(2)-C(1)	1.16(8)
C(2)-C(4)	1.431(7)	C(2)-C(4)	1.33(6)
C(7)-N(3)	1.144(6)	C(7)-N(3)	1.20(5)
C(7)-C(5)	1.428(6)	C(7)-C(5)	1.28(5)
N(4)-C(8)	1.141(6)	N(4)-C(8)	1.21(6)
C(5)-C(6)	1.363(6)	C(5)-C(6)	1.18(6)
C(1)-C(3)	1.429(6)	C(1)-C(3)	1.34(8)
C(8)-C(6)	1.436(6)	C(8)-C(6)	1.32(6)
C(3)-N(1)	1.142(6)	C(3)-N(1)	1.14(6)
N(5)-C(9)	1.322(6)	N(5)-C(9)	1.389(6)
N(5)-C(11)	1.343(6)	N(5)-C(15)	1.40(2)
N(5)-C(15)	1.473(7)	N(5)-C(11)	1.389(6)
N(6)-C(9)	1.288(6)	N(5)-C(10)	1.97(3)
N(6)-C(10)	1.354(6)	C(9)-N(6)	1.414(6)
N(6)-C(12)	1.474(7)	N(6)-C(10)	1.337(6)
C(11)-C(10)	1.329(7)	N(6)-C(12)	1.39(2)
C(12)-C(13)	1.366(8)	C(10)-C(11)	1.389(6)
C(14)-C(13)	1.504(8)	C(12)-C(13)	1.512(16)
C(17)-C(16)	1.406(8)	C(13)-C(14)	1.512(16)
C(15)-C(16)	1.397(13)	C(15)-C(16)	1.508(17)
		C(16)-C(17)	1.509(16)

Bond angles/°

T = 298 K		T = 368 K	
S(4)-Ni(1)-S(3)	92.3 (5)	S(4)-Ni(1)-S(3)	91.8(5)
S(4)-Ni(1)-S(1)	176.8 (7)	S(4)-Ni(1)-S(1)	179.3(5)
S(3)-Ni(1)-S(1)	88.1 (5)	S(3)-Ni(1)-S(1)	87.5(5)
S(4)-Ni(1)-S(2)	178.2 (5)	S(4)-Ni(1)-S(2)	88.5(5)
S(3)-Ni(1)-S(2)	86.8 (7)	S(4)-Ni(1)-S(1)	179.3(5)
S(1)-Ni(1)-S(2)	92.7 (5)	S(1)-Ni(1)-S(2)	92.3(5)
C(5)-S(3)-Ni(1)	103.4 (16)	C(5)-S(3)-Ni(1)	100(3)
C(1)-S(1)-Ni(1)	103.0 (17)	C(6)-S(4)-Ni(1)	101(3)

C(6)-S(4)-Ni(1)	103.3 (16)	C(2)-S(2)-Ni(1)	96(3)
C(2)-S(2)-Ni(1)	103.2 (17)	C(1)-S(1)-Ni(1)	103(3)
C(1)-C(2)-C(4)	121.4(4)	C(6)-C(5)-C(7)	122(8)
C(1)-C(2)-S(2)	120.7(4)	C(6)-C(5)-S(3)	125(8)
C(4)-C(2)-S(2)	117.9(4)	C(7)-C(5)-S(3)	113(6)
N(3)-C(7)-C(5)	179.0(5)	C(5)-C(6)-S(4)	121(8)
C(6)-C(5)-C(7)	121.2(4)	C(5)-C(6)-C(8)	122(8)
C(6)-C(5)-S(3)	120.5(4)	S(4)-C(6)-C(8)	116(5)
C(7)-C(5)-S(3)	118.2(3)	N(4)-C(8)-C(6)	179(6)
C(2)-C(1)-C(3)	121.2(4)	N(3)-C(7)-C(5)	179(6)
C(2)-C(1)-S(1)	120.3(4)	C(1)-C(2)-C(4)	128(9)
C(3)-C(1)-S(1)	118.5(4)	C(1)-C(2)-S(2)	130(9)
N(2)-C(4)-C(2)	178.9(5)	C(4)-C(2)-S(2)	103(6)
N(4)-C(8)-C(6)	178.3(5)	N(2)-C(4)-C(2)	166(6)
C(5)-C(6)-C(8)	120.1(4)	C(2)-C(1)-C(3)	124(8)
C(5)-C(6)-S(4)	120.5(3)	C(2)-C(1)-S(1)	119(9)
C(8)-C(6)-S(4)	119.5(3)	C(3)-C(1)-S(1)	117(6)
N(1)-C(3)-C(1)	179.3(6)	N(1)-C(3)-C(1)	175(8)
C(9)-N(5)-C(10)	109.7(7)	C(9)-N(5)-C(11)	108.0
C(9)-N(5)-C(12)	124.1(8)	C(9)-N(5)-C(15)	126.1(11)
C(10)-N(5)-C(12)	126.2(8)	C(11)-N(5)-C(15)	125.8(10)
C(9)-N(6)-C(11)	107.9(5)	N(5)-C(9)-N(6)	106.1
C(9)-N(5)-C(15)	125.2(6)	C(10)-N(6)-C(9)	109.5
C(11)-N(5)-C(15)	126.9(6)	C(10)-N(6)-C(12)	128.2(10)
C(10)-C(11)-N(6)	106.5(8)	C(12)-N(6)-C(9)	122.2(11)
N(6)-C(9)-N(5)	107.3(7)	N(6)-C(10)-C(11)	108.4
C(11)-C(10)-N(6)	107.2(8)	C(10)-C(11)-N(5)	108.0
C(13)-C(12)-N(6)	117.0(6)	N(6)-C(12)-C(13)	120(3)
C(14)-C(13)-C(12)	117.4(7)	C(14)-C(13)-C(12)	108(2)
C(16)-C(15)-N(5)	114.8(5)	N(5)-C(15)-C(16)	118(4)
C(15)-C(16)-C(17)	116.6(7)	C(15)-C(16)-C(17)	108(2)

Table S3 H-bonding in LTP and HTP output by Platon program

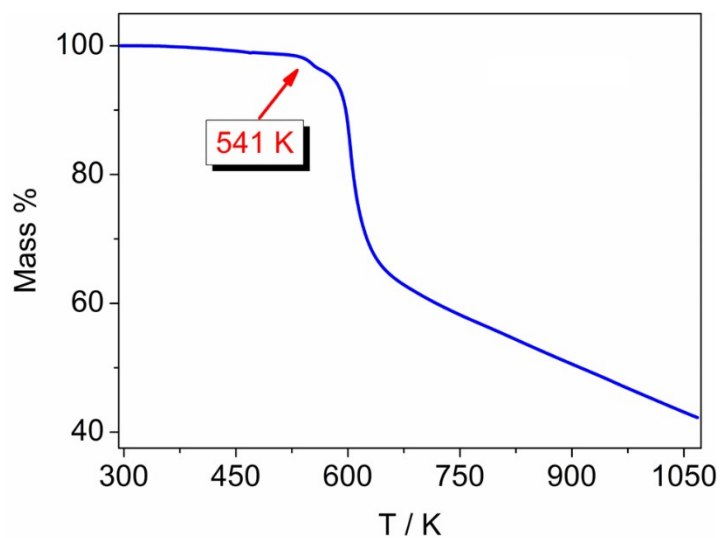|	LTP	HTP
Donor−H…Acceptor	C9–H9…N2	C11–H11…N3
D−H distance	0.93 Å	0.93 Å
H…A distance	2.61(4) Å	2.53(5) Å

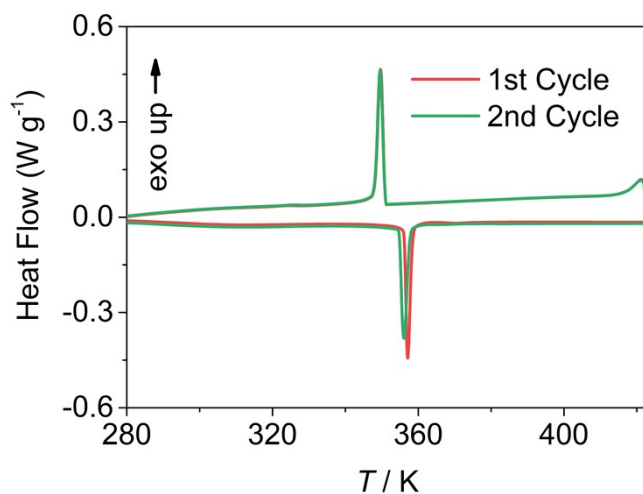Fig. S1. TG plot of **1** in 298−1073 K, and **1** is thermally stable up to ca.541 K, showing extra thermostability.

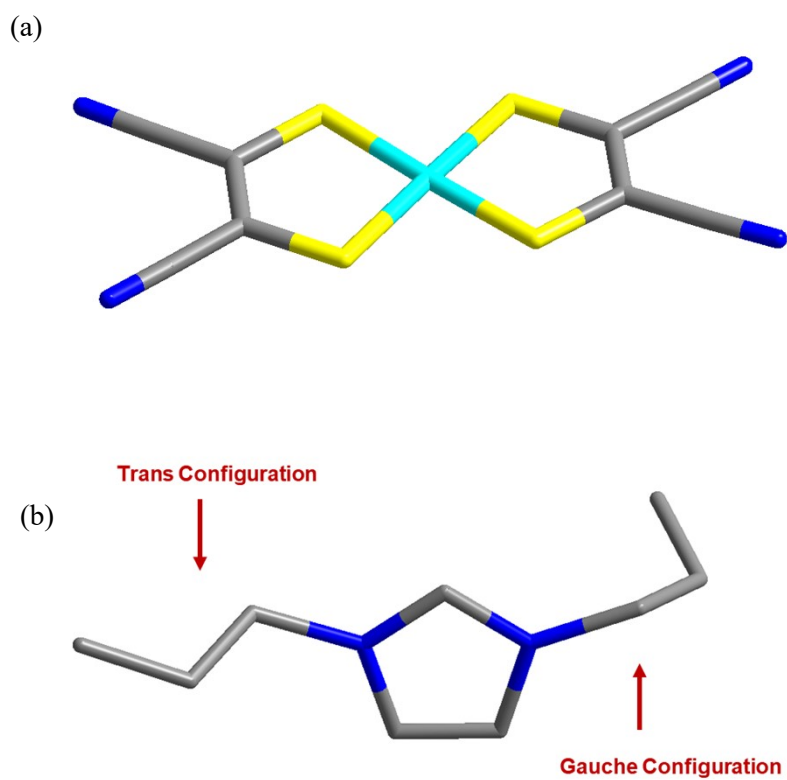Fig. S2. DSC plots of **1** in 280-423 K in two sequential heating-cooling cycles.

(a)

Trans Configuration

(b)

Gauche Configuration

Fig. S3. Illustration of (a) planar $[Ni(mnt)_2]^-$ anion and (b) $[DPIm]^+$ cation with different two configurations of alkyl chains.·
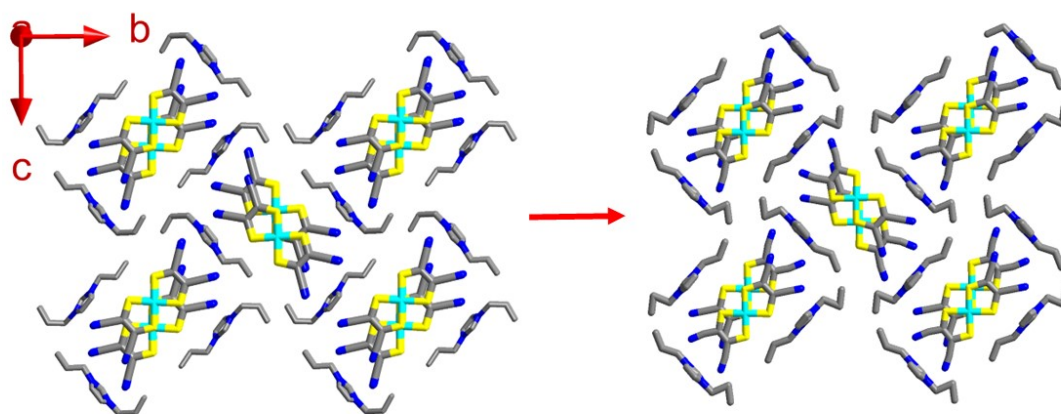

Fig. S4. The packing structure along a-axis view of LTP (left) and HTP (right).
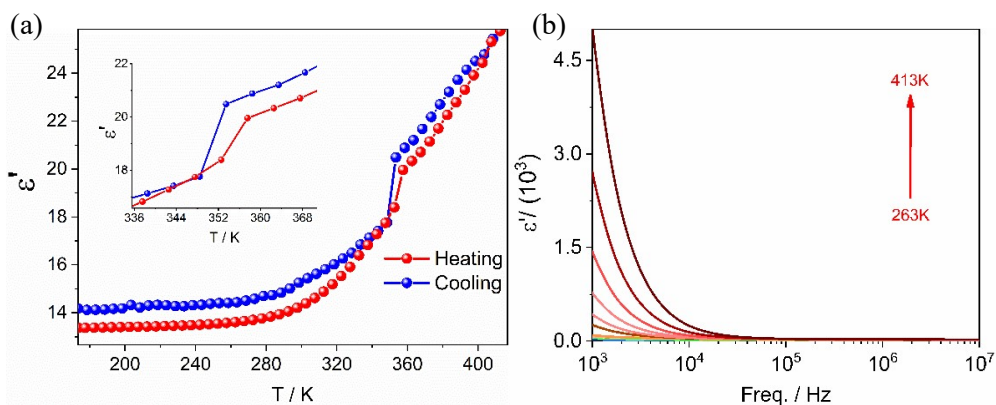
Fig. S5. (a) Plots of dielectric permittivity at frequency of 1 MHz in heating and cooling run, which exhibit the reversible low- and high-dielectric states of **1**. (b) Frequency dependent dielectric permittivity of **1** at the selected temperatures.
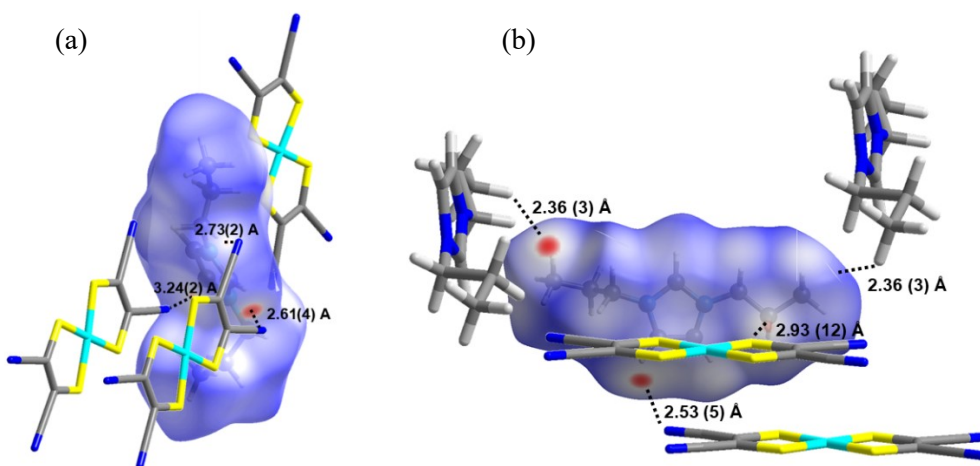

Fig. S6. Hirshfeld surface mapped with d_{norm}. Neighboring anions associated with close contacts are shown along with distances between the atoms involved for **1** in (a) LTP and (b) HTP.
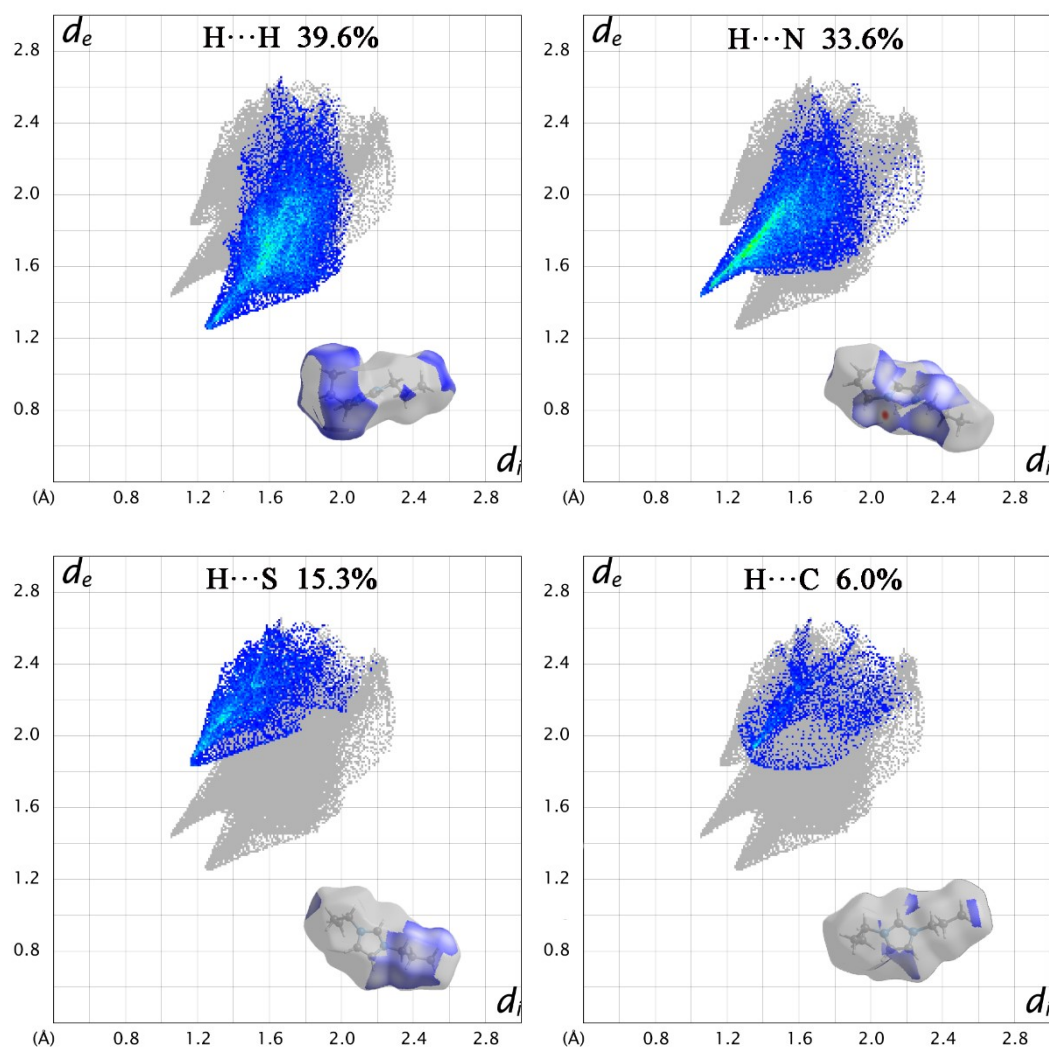
Fig. S7. The Hirshfeld d$_{norm}$ surfaces and the 2D fingerprint plots of close contacts the thiomorpholine cations in LTP of **1**.
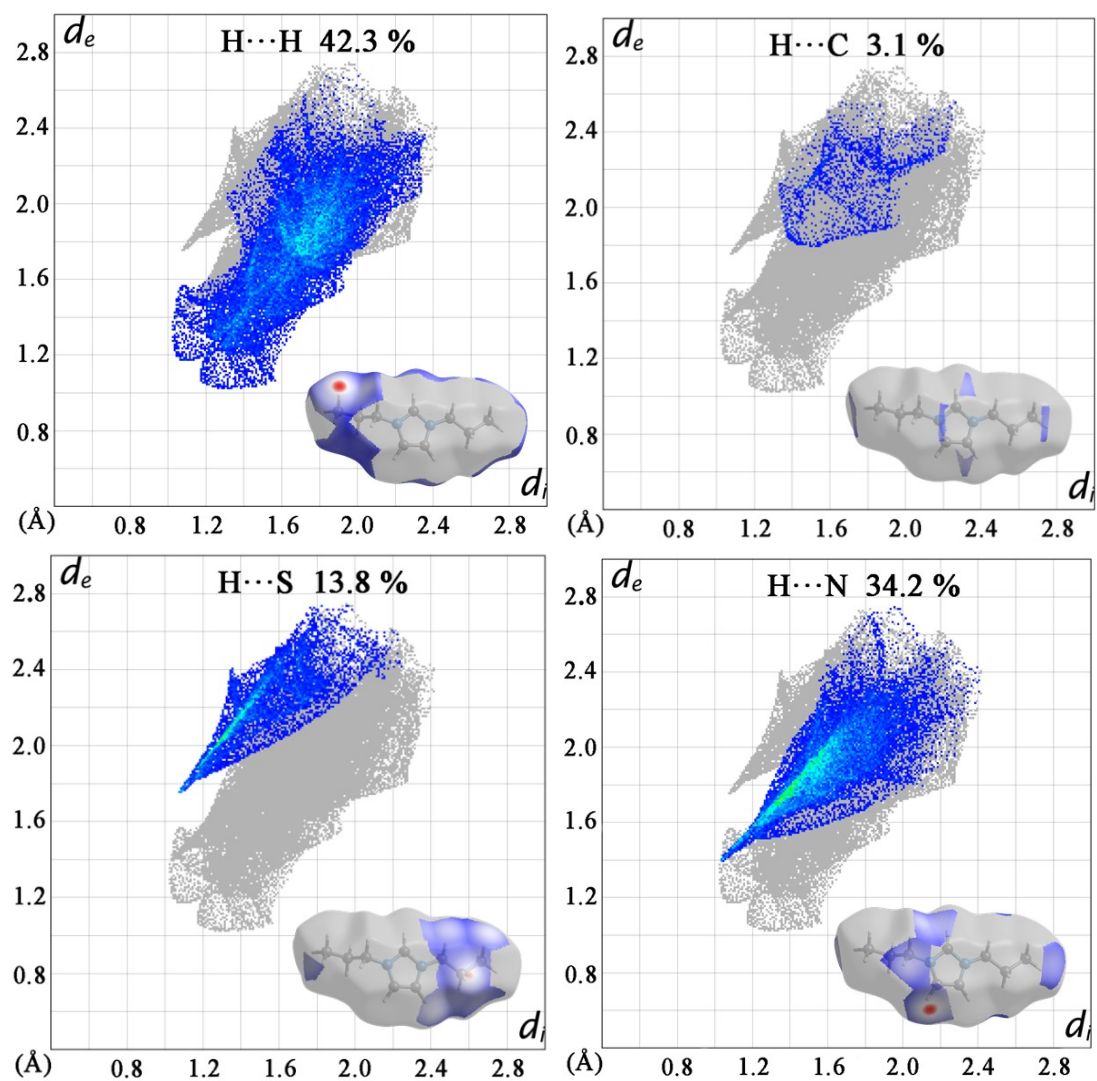
Fig. S8. The Hirshfeld d_{norm} surfaces and the 2D fingerprint plots of the thiomorpholine cations in HTP of **1**.

References

1. A. Davidson, H. R. Holm, *Inorg. Synth.* **1967**, *10*, 8−26.

2. Bruker. *APEX 2, SAINT, XPREP*; Bruker AXS Inc.: Madison, Wisconsin, USA, 2007.

3. Bruker. *SADABS*; Bruker AXS Inc.: Madison, Wisconsin, USA, 2001.

4. G. M. Sheldrick, SHELXS-2014, Program for the Solution and Refinement of Crystal Structures; University of Göttingen: Göttingen, Germany, 2014.